# Equation of state of the α-PbO_{2} and Pa3[over ¯]-type phases of GeO_{2} to 120 GPa

R. Dutta, C. E. White, E. Greenberg, V. B. Prakapenka, and T. S. Duffy

Phys. Rev. B **98**, 144106 — Published 11 October 2018

DOI: 10.1103/PhysRevB.98.144106

# Equation of state of the α-$PbO_2$ and $Pa\bar{3}$-type phases of germania, $GeO_2$, to 120 GPa

R. Dutta[1*], C. E. White[2, 3], E. Greenberg[4], V. B. Prakapenka[4] and T. S. Duffy[1]

[1]Department of Geosciences, Princeton University, NJ 08544, USA.
[2]Department of Civil and Environmental Engineering, Princeton University, NJ 08544, USA.
[3]Andlinger Center for Energy and the Environment, Princeton University, NJ 08544, USA.
[4]Center for Advanced Radiation Sources, University of Chicago, Chicago, IL 60637, USA.

**Abstract**

The compression behavior of crystalline and amorphous germania holds considerable interest as an analog for silica and for understanding the structural response of $AX_2$ compounds generally. In this work, the α-$PbO_2$-type and $Pa\bar{3}$-type polymorphs of $GeO_2$ were investigated under high pressure using angle-dispersive synchrotron x-ray diffraction in the laser-heated diamond anvil cell. Theoretical calculations based on density functional theory were also performed. The experimental pressure-volume data were fitted to 3rd order Birch-Murnaghan equations of state. The fit parameters for the α-$PbO_2$-type are: $V_0$ = 53.8 (2) Å$^3$, $K_{0T}$ = 293 (7) GPa with fixed $K'_{0T} = 4$; where $V$, $K_T$, and $K'_T$ are the volume, isothermal bulk modulus, and pressure derivative of the bulk modulus and the subscript 0 refers to ambient conditions. The corresponding parameters for the $Pa\bar{3}$-type phase is: $V_0$ = 50.3 (3) Å$^3$, $K_{0T}$ = 342 (12) GPa with fixed $K'_{0T} = 4$. The theoretical calculations are in good agreement with the experimental results with slight underestimation and overestimation of $V_0$ and $K_{0T}$ respectively. A theoretical Hugoniot was calculated from our data and compared to shock equation of state data for vitreous and rutile-type $GeO_2$. The high-pressure phase observed on the Hugoniot is most consistent with either the α-$PbO_2$-type or $CaCl_2$-type phase. Finally, we have compared our data on crystalline germania with existing studies on the corresponding phases of $SiO_2$ to better understand the effects of cation substitution on phase transformations and equations of state in Group 14 dioxides.

## Introduction

The crystalline and vitreous forms of germania, $GeO_2$ have been extensively studied using a wide range of static and dynamic compression techniques[1–3]. The structure of amorphous germania at high pressure has been examined using x-ray absorption spectroscopy[4–7], Raman[8] and Infrared spectroscopy[9] as well as x-ray[10–13] and neutron diffraction[14–16]. Static compression experiments on crystalline $GeO_2$ have concentrated on the high-pressure crystal structure[17–19] and phase transitions[20–22]. Dynamic compression experiments[1,2,23–25] have also been carried out on germania crystals and glass. There have also been a number of theoretical studies[26–29] investigating the high-pressure behavior of the different phases of this material.

The long-standing interest in $GeO_2$ is due in part to its role as a structural analog for $SiO_2$. Silica is the most abundant oxide component of the earth's crust and mantle. High-pressure experiments and theoretical calculations show that the phase transition sequence in $SiO_2$, starting from rutile-type (stishovite) is $CaCl_2$-type[30,31] (60 GPa) – α-$PbO_2$-type (seifertite)[32] (121 GPa) – $Pa\overline{3}$-type[33] (sometimes referred to as pyrite-type) (268 GPa). Density functional calculations have predicted a further transition from the $Pa\overline{3}$-type structure to a $Fe_2P$-type[34] structure at 640 GPa or cotunnite[35] (α-$PbCl_2$)-type structure around 700 GPa. Although, the ultra-high-pressure phases are not expected to be stable in the Earth's interior, they may be key components of large, rocky extra-solar planets[36]. A large number of additional studies[37–41] have also focused on the high-pressure behavior of silica glass to understand the structural and coordination number changes it undergoes as a function of static and dynamic compression.

The extreme pressures required for phase transitions in $SiO_2$ make it very challenging to study many of these phases experimentally, necessitating the use of analogs[3,42–44]. At pressures above a megabar (100 GPa), it is difficult to maintain thermally uniform conditions in laser-

heated diamond anvil cells. $GeO_2$ follows a similar sequence of phase transitions as $SiO_2$, but the phase transitions occur at lower pressures due to the larger ionic radius of $Ge^{4+}$ compared with $Si^{4+}$. This facilitates the use of thicker samples and insulating layers in the diamond anvil cell and more controlled heating conditions.

Under room-temperature compression, α-quartz-type germania has been reported to undergo pressure-induced amorphization[45] or form a disordered monoclinic ($P2_1/c$) phase above 6 GPa[18]. Rutile-structured germania (*P42/mnm*) undergoes a phase transition to the orthorhombic $CaCl_2$-type (*Pnnm*) near 26 GPa with a positive Clapeyron slope[20]. This is followed by transitions to the α-$PbO_2$-type (*Pbcn*) phase near 36 GPa[21] and the $Pa\overline{3}$-type phase near 65 GPa[26] (theory) or 90 GPa[46]. No further phase transitions are observed up to 130 GPa[19]. First-principles calculations[29] predict the $Pa\overline{3}$-type to cotunnite-type and cotunnite-type to $Fe_2P$-type phase transitions to occur at ~300 GPa and ~600 GPa respectively.

For glasses and liquids, $GeO_2$ is used to model the response of tetrahedral-network glasses and their evolution from corner-sharing tetrahedra at ambient pressure to a dense octahedrally coordinated glass at high pressures[7,10,47]. It has been suggested based on molecular dynamics simulations that $GeO_2$ glass undergoes multiple amorphous-amorphous transitions that have direct parallels to their crystalline counterparts under pressure[48]. Recent extended x-ray absorption fine structure (EXAFS) and x-ray absorption near edge structure (XANES) spectra on dense $GeO_2$ glass show evidence for changes in bond distance and coordination number increase at high pressure above 45 GPa[7]. Shock-wave compression of vitreous and crystalline rutile-type $GeO_2$ suggest a common high-pressure phase (hpp) or a phase with ~5% higher zero-pressure density (with respect to rutile) above 35 GPa and 70 GPa, respectively[1].

Much of the existing work on high-pressure $GeO_2$ crystalline phases is fragmentary, and there is limited experimental data above 50 GPa. In this study, we have performed laser-heated diamond anvil cell (LHDAC) experiments and *ab initio* calculations to obtain the 300-K (0 K for theoretical calculations) equation of state (EOS) of the α-$PbO_2$- and $Pa\overline{3}$-type phases of $GeO_2$ to 120 GPa. We have compared our pressure-volume data with previous studies for both $SiO_2$ and $GeO_2$. We have also compared our results with shock compression data to better identify possible candidates for the high-pressure Hugoniot phase(s).

## A. Experimental Procedure

Polycrystalline $GeO_2$ (Aldrich, >99.998% purity) was examined at ambient conditions using synchrotron x-ray diffraction and was found to be in the α-quartz structure with lattice parameters $a$ = 4.963 (1) Å, $c$ = 5.638 (3) Å, in good agreement with literature values[49]. The sample was ground to micron-sized grains under ethanol and mixed with 10 wt% platinum to serve as both the pressure calibrant and laser absorber. The sample + Pt mixture was then pressed into ~ 7-10 μm thick foils. Rhenium gaskets were pre-indented to ~20-30 μm thickness and 60-120-μm diameter holes were drilled to form the sample chamber. The sample foils were then loaded into symmetric diamond anvil cells with 100-200 μm culet diamond anvils mounted on WC or cubic BN seats. Three ruby balls (~5-μm diameter) arranged in a triangular pattern were used to support the sample. Neon was loaded into the sample chamber using the gas-loading system at GeoSoilEnviroCARS (GSECARS), Sector 13 of the Advanced Photon Source (APS). Pressure was determined using the (111) diffraction peak and the EOS of Pt[50,51].

*In situ* angle-dispersive x-ray diffraction was carried out at beamline 13-ID-D of the APS using a monochromatic x-ray beam (λ = 0.3344 Å). The x-rays were focused to a ~3 μm x 3 μm spot size using Kirkpatrick-Baez mirrors. Diffraction patterns were collected using a two-

dimensional 165 MAR-CCD or a CdTe 1M Pilatus detector. Lanthanum hexaboride ($LaB_6$) was used as a standard to calibrate the detector position and orientation.

X-ray diffraction patterns were collected at 1-5 GPa intervals for 5-30 seconds. High-pressure phases were synthesized by heating from both sides using diode pumped fiber lasers[52] with a ~15 μm spot size. The sample was annealed at ~1200 K after each ~5 GPa pressure step to relax differential stress. Temperatures were measured using spectroradiometry[53]. The laser power on each side was adjusted independently so that temperature differences between the upstream and downstream sides were less than 50 K. The 2D images were integrated to obtain the one-dimensional x-ray patterns using the software DIOPTAS[54]. Peak positions were determined by fitting background-subtracted Voigt shapes to the data. Lattice parameters were calculated using least-squares refinement of the peak positions using the program UnitCell[55].

**B. Computational details**

Total energy calculations were performed using the plane wave implementation of density functional theory[56,57] (DFT) as implemented in the CASTEP[58] code. The exchange and correlation energies were treated using the local density approximation (LDA). For all calculations, we used a kinetic energy cutoff of 400 eV for the basis set. The Brillouin zone was sampled using a Monkhorst-Pack[59] 4x3x3 and 4x4x4 $k$-point grid for the α-$PbO_2$ and $Pa\overline{3}$-type phases, respectively. Ultrasoft[60] pseudopotentials were used to treat the electron-ion interactions. The geometry optimizations were carried out using the Broyden-Fletcher-Goldfarb-Shanno[61] algorithm and were considered complete when the forces on atoms were less than 0.01 eV/ Å and the energy change was less than 5 x $10^{-6}$ eV/atom. Both atomic positions and lattice parameters were optimized at each pressure step.

## C. Data Analysis

The pressure-volume data for the different phases were fit to an isothermal 3rd order Birch-Murnaghan (BM-3) EOS:

$$P(V) = \frac{3}{2}K_{0T}\left[\left(\frac{V_0}{V}\right)^{\frac{7}{3}} - \left(\frac{V_0}{V}\right)^{\frac{5}{3}}\right]\left\{1 + \frac{3}{4}(K'_{0T} - 4)\left[\left(\frac{V_0}{V}\right)^{\frac{2}{3}} - 1\right]\right\}, \quad (1)$$

where $P$ is the pressure, $K_T$ is the isothermal bulk modulus, $K'_T$ is the pressure derivative of the bulk modulus, $V$ is the unit cell volume and the subscript 0 refers to ambient pressure. For the experimental data, $K'_{0T}$ was fixed at 4 in performing the fit.

The presence of non-hydrostatic stresses can affect equation of state determination in a diamond anvil cell. To assess this, the differential stresses in the Pt pressure standard were evaluated using lattice strain theory[62]. Differential stress (t) results in variation in the lattice dimension as a function of crystallographic orientation (*hkl*) for elastically anisotropic crystals. For a crystal with cubic symmetry, the elastic anisotropy can be expressed using the anisotropy factor, *S*:

$$S = \left(\frac{S_{11} - S_{12} - S_{44}}{2}\right), \quad (2)$$

where *Sij* are the single-crystal elastic compliances. The effect of deviatoric stress on the measured unit cell parameter, $a_m$, for a given (*hkl*) can be expressed as[62,63]:

$$a_m(hkl) = M_0 + M_1[3(1 - 3sin^2\theta)\Gamma(hkl)], \quad (3)$$

where,

$$M_0 = a_P\left(1 + \frac{\alpha t}{3}(1 - 3sin^2\theta)\left[S_{11} - S_{12} - \frac{1 - \alpha^{-1}}{2G_V}\right]\right), \quad (4)$$

$$M_1 = -\frac{a_P \alpha St}{3}, \qquad (5)$$

$$\Gamma(hkl) = \frac{h^2k^2 + k^2l^2 + l^2h^2}{(h^2 + k^2 + l^2)^2}. \qquad (6)$$

$a_P$ is the lattice parameter under hydrostatic pressure ($P$) only, α is a measure of continuity of stress and strain across grain boundaries and $\theta$ is the scattering angle; α typically takes values between 0.5 and 1 but it has been suggested that it can exceed one in certain cases[64]. $G_v$ is the Voigt limit of the shear modulus under iso-strain conditions. Assuming, $M_0 \approx a_P$ and α = 1 (Ref: 49, 53), the product $St$ can be derived directly from the slope and intercept of the Γ-plot [$a_m(hkl)$ vs $3(1 - 3sin^2\theta)\Gamma(hkl)$]:

$$St \approx \frac{3M_1}{M_0}. \qquad (7)$$

The anisotropy factor of platinum as a function of pressure was obtained from theoretical calculations of Menéndez-Proupin and Singh, 2007 (Ref. 66).

We have also calculated a theoretical Hugoniot for $GeO_2$ using our experimental 300-K isotherm and the Mie-Grüneisen equation[67]. For any volume of interest, $V$, we compute the pressure along the principal isentrope, $P_S(V)$, and then we isochorically determine the difference in pressure between the isentrope and the Hugoniot using:

$$P_H(V) = \frac{\left\{P_S(V) - \frac{\gamma}{V}(\Delta E_S + E_{TR})\right\}}{\left\{1 - \left(\frac{\gamma}{2}\right)\left(\frac{V_{00}}{V} - 1\right)\right\}}, \qquad (8)$$

where, $P_H$, $V_{00}$, γ and $E_{TR}$ are the Hugoniot pressure, initial volume of the shocked material, the Grüneisen parameter and the phase transition energy at ambient pressure. The volume dependence of the Grüneisen parameter is assumed to be given by:

$$\gamma = \gamma_0 (V/V_0)^q, \qquad (9)$$

In our calculations, we have used $q$ = 1 and $\gamma_0$ between 1 and 2. The energy change along the principal isentrope ($\Delta E_S$) is evaluated by numerically integrating:

$$\Delta E_S = -\int_{V_0}^{V} P_S dV. \qquad (10)$$

The principal isentrope was assumed to have the form of the 3rd order Birch Murnaghan.

$K_S$, the isentropic bulk modulus and $K_S'$, its pressure derivative is assumed to be related to the isothermal counterparts, $K_T$ and $K_T'$ using:

$$K_S = K_T(1 + \alpha\gamma T), \qquad (11)$$

$$\left(\frac{\partial K_s}{\partial P}\right)_T \approx (1 + \alpha\gamma T)K_T' + \frac{\gamma T}{K_T}\left(\frac{\partial K_T}{\partial T}\right)_P, \qquad (12)$$

$$K_T' = \left(\frac{\partial K_T}{\partial P}\right)_T, \qquad (13)$$

$$K_S' = \left(\frac{\partial K_S}{\partial P}\right)_S = \left(\frac{\partial K_s}{\partial P}\right)_T + \left(\frac{\partial K_s}{\partial T}\right)_P \frac{\gamma T}{K_S}. \qquad (14)$$

## Results

### Equation of State

A $GeO_2$ sample was compressed at room temperature to 50.4 GPa. The 300-K diffraction pattern was consistent with a poorly crystalline monoclinic phase ($P2_1/c$) previously reported[18,22]. Upon heating to ~1700 K, new diffraction peaks appeared, and these peaks were retained upon quenching to room temperature after 30 minutes of heating time (*in situ* P = 51.0 GPa, Fig. 1). The measured *d*-spacings could be fit to the α-$PbO_2$-type structure (suppl. material[68]; Table S1) which is the expected stable phase at these pressures[21]. The difference between our observed and calculated *d*-spacings are less than < 0.003 Å, indicating a good fit to the α-$PbO_2$-type structure. We then increased the pressure in 1-5 GPa steps with annealing at 1200 K (for ~5 minutes) at ~5-GPa intervals. Annealing was designed to reduce the differential stress. Figure 2 shows the lattice parameters obtained from both the experiments and theoretical calculations as a function of pressure up to 95 GPa. As expected, LDA underestimates the unit cell dimensions with respect to experimentally obtained values. Our measured values are in good agreement with existing literature[46,69]. The experimental *a*, *b* and *c* axial dimensions were found to decrease by 2.4, 2.6 and 2.3% respectively in the pressure range considered. The theoretically calculated parameters on the other hand decrease by 2.7, 2.1 and 2.1% between 50 and 90 GPa. However, the volume reduction obtained from the two methods are in good agreement (7.1 and 6.9% using experiments and theory respectively).

Figure 3 shows the pressure-volume relation of α-$PbO_2$-type $GeO_2$. The EOS parameters are shown in Table 1. Figure 4 (solid black lines) shows the co-variance between $K_{0T}$ and $V_0$ in the fitting results (1σ, 68.3 % confidence). The negative slope of the confidence ellipse indicates

the strong negative correlation between $K_{0T}$ and $V_0$. The error bars indicate the estimated standard deviations of the two parameters.

We have examined the dependence of the fitting parameters on the choice of EOS of the platinum pressure standard. The EOS of Dewaele et al. 2004 (Ref. 51) and Fei et al. 2007 (Ref. 50) used as our primary pressure calibration is based on DAC data and cross-calibration of multiple standards up to 94 GPa. On the other hand, the pressure scale of Dorfman et al. 2012 (Ref. 65) (data fit to BM-3) is calibrated over high pressures (to 250 GPa) using the MgO scale[70]. Using this EOS[65], we find that $V_0$ is 0.1% lower, while $K_{0T}$ is 4.1% higher. Although not significantly different from our initial fitting parameters (Table 1); it illustrates how modest differences in EOS parameters for standards affect the final EOS of the material under study. The $V_0$ vs $K_{0T}$ tradeoff curve for this case is also shown in figure 4 (red dashed lines).

An equation of state fit was also performed for the theoretical results both with and without fixing $K'_{0T}$. Table 2 lists the EOS parameters obtained from experiments and theory from this work and previous studies on $GeO_2$ and $SiO_2$. Using $K'_{0T} = 4$ for both the experimental and theoretical data, LDA was found to underestimate $V_0$ by 4.0% and overestimate $K_{0T}$ by 4.6%. Our estimated $K_{0T}$ values (293 GPa and 291 GPa using experiments and theory, respectively) are higher than reported by Prakapenka et al. 2003 (Ref. 69) which was based on more limited pressure range (to 60 GPa) and lacked a pressure-transmitting medium.

A fresh sample was then prepared and compressed to 80.0 GPa at room-temperature. Again, the ambient-temperature diffraction pattern could be assigned to the $P2_1/c$ monoclinic phase. On heating at ~1690 K, new x-ray diffraction peaks were observed. The temperature-quenched diffraction pattern after 20 minutes heating could be indexed using the $Pa\bar{3}$-type

structure (see suppl. Material, Table S2). Figure 5 shows the diffraction pattern obtained on quenching from the peak temperature (*in situ* P = 82.8 GPa). The sample was then further compressed to 119.5 GPa resulting in a 1.7 % decrease in unit cell parameter over this range. The LDA calculations systematically underestimate the lattice parameter as also observed for the α-$PbO_2$-type phase. However, theory and experiment show a similar pressure dependence as the theoretically calculated lattice parameter decreases by 1.8 % between 80 and 120 GPa. Figure 6 shows the pressure-volume relation obtained from this work as well as limited data available from previous experimental studies[19,46]. Using a 3rd order Birch Murnaghan fit to our experimental data, the EOS parameters are $V_0$ = 100.6 (5) Å$^3$, $K_{0T}$ = 342 (12) GPa and $K'_{0T}$ = 4 (fixed). At 108 GPa, our cell volume (81.68 Å$^3$) is in good agreement with Shiraki et al. 2003 (Ref. 19) (81.54 Å$^3$) and Ono et al. 2003 (Ref. 46) (81. 48 Å$^3$). Figure 8 shows the co-variance (1σ) of $K_{0T}$ and $V_0$ for the experimental data. In case of the theoretical data, $V_0$ and $K_{0T}$ are underestimated and overestimated by 3.9% and 2.7% respectively. Table 1 summarizes the EOS parameters obtained from both experiments and theory and compares it to available experimental and theoretical data. Figure 7 shows the correlation ellipses for $V_0$ and $K_{0T}$ using the platinum EOS parameters of Dewaele et al. 2004 (Ref. 51) and Fei et al. 2007 (Ref. 50) (solid black) and Dorfman et al. 2012 (Ref. 65) (red dashed). In the latter case, the fitting parameters $V_0$ and $K_{0T}$ are 0.1% and 4.1% higher and lower respectively.

**Differential Stress**

Figure 8 shows an example of variation of the measured lattice parameter ($a_m$) with $3(1-3sin^2\theta)\Gamma(hkl)$ for Pt at 113.8 GPa. The data points can be fit well using a straight line. The negative slope of the line is consistent with the orientation of anisotropy in Pt[66], and thus the variations in lattice parameter are consistent with effects of differential stress. Using the slope

and intercept of the Γ-plots, we calculated the differential stress as a function of pressure and compared it with previous experiments on Pt in Ne medium[65] and without any medium[71] (Figure 9). The differential stress increases with pressure from ~0.7 GPa at 52 GPa to ~2.6 GPa at the peak pressure (119.5 GPa).

Our results are consistent with previous work on Pt using a Ne medium[65] and lie below reported values of $t$ when no medium is used[71]. This indicates that Pt has not yet reached its yield point, so our values provide a reasonable estimate of the differential stress in the sample. In general agreement with previous observations[65] $t$ is ~2% of the total pressure at Mbar conditions. The low differential stress in platinum indicates that quasi-hydrostatic conditions were maintained in the DAC up to the peak pressure. The effects of laser annealing can also be observed in this data as differential stress tends to drop immediately after laser heating (Fig. 9). Differential stresses could not be directly evaluated in the cubic phase of $GeO_2$ due to lack of reported single-crystal elasticity data.

**Comparison with Shock Compression data**

The behavior of $GeO_2$ under dynamic compression has also attracted interest [1,2,24,25,72]. Gas gun shock-wave experiments[1] on rutile-type and amorphous $GeO_2$ have been interpreted to indicate a phase transition to a high-pressure phase at P > 70 GPa and >35 GPa, respectively. However, the structure of the hpp could not be directly determined in these experiments.

Figure 10 shows the theoretical Hugoniots assuming the rutile phase as an initial state and transforming to the different possible high-pressure phases of $GeO_2$. The Hugoniot of $SiO_2$ stishovite[73] is shown for comparison. The parameters used for the calculations are summarized in Table 2. In agreement with Jackson and Ahrens, 1979 (Ref. 1), the low-pressure region (up to

~50 GPa) can be well described with the rutile-type phase and thus there is no evidence of a phase transition up to this pressure. The data at 70-90 GPa are generally consistent with a theoretical Hugoniot calculated assuming either the $CaCl_2$- or the α-$PbO_2$-type phase as the hpp. The highest-pressure datum (165.5 GPa) is not consistent with the predicted Hugoniots of any of the high-pressure phases of $GeO_2$ and may represent melt. The $Pa\overline{3}$-type phase can be ruled out as a candidate hpp as it is predicted to be much denser along the Hugoniot than the experimental data.

**Discussion**

The data reported here provide detailed 300-K equations of state for the high-pressure α-$PbO_2$- and $Pa\overline{3}$-type phases of $GeO_2$. Our results are consistent with limited previous data and enable us to constrain EOS parameters for these materials. The equations of state of $GeO_2$ phases provide a benchmark for theoretical calculations and are of interest for comparison with the behavior of $SiO_2$ (see below). Crystalline $GeO_2$ equation of state data also have applications in interpretation of experimental studies of $GeO_2$ glass by x-ray absorption spectroscopy[4,7] and x-ray diffraction[13] as well as by theoretical molecular dynamics simulations[48].

Figure 11 compares the measured 300-K pressure-volume relationships across four phases of $GeO_2$ and $SiO_2$[74–76]. Because of the larger size of the $Ge^{4+}$ cation in comparison to $Si^{4+}$, $GeO_2$ has a larger unit cell volume but $SiO_2$ and $GeO_2$ follow the same phase transition sequence. The rutile (stishovite) to $CaCl_2$-type phase transition is second-order[74,77] with almost no volume change. A detailed study of the equation of state of the rutile and $CaCl_2$-type phases of $GeO_2$ will be published separately[78]. In the case of $SiO_2$, the $CaCl_2$ to α-$PbO_2$-type phase transition leads to a 0.6% reduction in molar volume[32], while the α-$PbO_2$-type to $Pa\overline{3}$-type phase

transition involves a 5% volume change[33]. Using our equation of state parameters, we determine the volume change to be 1.9% and 1.3% for the $CaCl_2$-type to α-$PbO_2$-type transition from experiments and theory, respectively (assuming transition pressure = 36 GPa). In case of the α-$PbO_2$-type to $Pa\overline{3}$-type transition, the volume reduction is 4.8% and 4.9% for experiments and theory, respectively (assuming transition pressure = 65 GPa) which is similar to the volume change in $SiO_2$.

Table 1 lists the EOS parameters for the α-$PbO_2$- and $Pa\overline{3}$-type phases of both $SiO_2$ and $GeO_2$ from both experiments and theoretical calculations. For the α-$PbO_2$-type phase, the zero-pressure bulk modulus of $GeO_2$ is ~9% lower than that of the $SiO_2$ phase. However, the experimental data suggest that the bulk moduli of $GeO_2$ and $SiO_2$ in the $Pa\overline{3}$-type phase may be more similar. Based on our experimental equation of state date, the zero-pressure bulk modulus of the $Pa\overline{3}$-type phase is about 16% larger than that of the α-$PbO_2$-type phase.

Shock compression experiments on fused silica and α-quartz indicate transitions to stishovite and/or stishovite-like phase(s) at ~35 GPa[41,79] with melting occurring above ~70 GPa and ~110 GPa respectively[80]. Direct shock compression experiments[73] on stishovite starting material do not show any evidence for phase transitions up to ~235 GPa. We calculated the theoretical Hugoniot of the different phases of $GeO_2$ based on rutile-type staring material. Our calculations suggest that the high-pressure phase observed on shock compression of vitreous and rutile-type germania can be interpreted as either the $CaCl_2$- or α-$PbO_2$-type phase.

**Conclusions**

Using laser-heated diamond anvil cell experiments and theoretical calculations based on density functional theory, we have determined the lattice parameter(s) of α-$PbO_2$- and $Pa\overline{3}$-type

$GeO_2$ up to 1.2 Mbar. The pressure-volume data were fit to the 3rd order Birch-Murnaghan equation of state. Our experimental and theoretical data are in good agreement. The experimental and theoretical data for the α-$PbO_2$-type phase can be fit using $V_0$ = 53.8 (2) Å$^3$, $K_{0T}$ = 293 (7) GPa and $V_0$ = 51.6 Å$^3$, $K_{0T}$ = 307 GPa; $K'_{0T} = 4$(fixed) respectively. In case of the $Pa\overline{3}$-type phase, the EOS parameters obtained from fitting the experimental and theoretical data are $V_0$ = 50.3 (3) Å$^3$, $K_{0T}$ = 342 (12) GPa and $V_0$ = 48.3 Å$^3$, $K_{0T}$ = 351 GPa; $K'_{0T} = 4$(fixed) respectively. Non-hydrostatic stress analysis of Pt shows that the differential stress in the cells were low (~2% at the peak pressure) and quasi-hydrostatic conditions were maintained. The effect of choosing different Pt pressure standards on the equation of state of $GeO_2$ has also been evaluated.

**Acknowledgements**

The authors are grateful to S. J. Tracy, C. V. Stan, J. K. Wicks and S. Tkachev for helpful comments on the manuscript and/or experimental assistance. The work was funded by the National Science Foundation (EAR-1415321). Use of the Advanced Photon Source, an Office of Science User Facility, U.S. Department of Energy is acknowledged. GeoSoilEnviroCARS (GSECARS, Sector 13), is supported by the NSF Earth Sciences (Grant No: EAR-1634415) and the Department of Energy, Geosciences (Grant No. DE-FG02-94ER14466). The gas-loading facility at GSECARS is partially supported by the Consortium for Materials Properties Research in Earth Sciences under NSF Cooperative Agreement EAR 1606856. This research used resources of the Advanced Photon Source, a U.S. Department of Energy (DOE) Office of Science User Facility operated for the DOE Office of Science by Argonne National Laboratory under Contract No. DE-AC02-06CH11357.

## References


[1] I. Jackson and T.J. Ahrens, Phys. Earth Planet. Inter **20**, 60 (1979).

[2] C. Liu, T.J. Ahrens, and N.S. Brar, J. Appl. Phys **91**, 9136 (2002).

[3] M. Micoulaut, L. Cormier, and G.S. Henderson, J. Phys.: Condens. Matter **18**, R753 (2006).

[4] X. Hong, G. Shen, V.B. Prakapenka, M. Newville, M.L. Rivers, and S.R. Sutton, Phys. Rev. B **75**, 104201 (2007).

[5] M. Vaccari, G. Aquilanti, S. Pascarelli, and O. Mathon, J. Phys.: Condens. Matter **21**, 145403 (2009).

[6] M. Baldini, G. Aquilanti, H. Mao, W. Yang, G. Shen, S. Pascarelli, and W.L. Mao, Phys. Rev. B **81**, 024201 (2010).

[7] X. Hong, M. Newville, T.S. Duffy, S.R. Sutton, and M.L. Rivers, J. Phys.: Condens. Matter **26**, 035104 (2014).

[8] D.J. Durben and G.H. Wolf, Phys. Rev. B **43**, 2355 (1991).

[9] P.V. Teredesai, D.T. Anderson, N. Hauser, K. Lantzky, and J.L. Yarger, Phys. Chem. Glasses **46**, 345 (2005).

[10] M. Guthrie, C.A. Tulk, C.J. Benmore, J. Xu, J.L. Yarger, D.D. Klug, J.S. Tse, H. Mao, and R.J. Hemley, Phys. Rev. Lett. **93**, 115502 (2004).

[11] Q. Mei, S. Sinogeikin, G. Shen, S. Amin, C.J. Benmore, and K. Ding, Phys. Rev. B **81**, 174113 (2010).

[12] G. Lelong, L. Cormier, G. Ferlat, and V. Giordano, High Pressure Studies Using Synchrotron Radiation: Present and Future, Synchrotron SOLEIL (France) (2012).

[13] Y. Kono, C. Kenney-Benson, D. Ikuta, Y. Shibazaki, Y. Wang, and G. Shen, Proc. Natl. Acad Sci. U. S. A **113**, 3436 (2016).

[14] J.A. Erwin Desa, A.C. Wright, and R.N. Sinclair, J. Non-Cryst. Solids **99**, 276 (1988).

[15] J.W.E. Drewitt, P.S. Salmon, A.C. Barnes, S. Klotz, H.E. Fischer, and W.A. Crichton, Phys. Rev. B **81**, 014202 (2010).

[16] P.S. Salmon, J.W.E. Drewitt, D.A.J. Whittaker, A. Zeidler, K. Wezka, C.L. Bull, M.G. Tucker, M.C. Wilding, M. Guthrie, and D. Marrocchelli, J. Phys.: Condens. Matter **24**, 415102 (2012).

[17] J. Haines, J.M. Léger, C. Chateau, and A.S. Pereira, Phys. Chem. Min **27**, 575 (2000).

[18] J. Haines, J.M. Léger, and C. Chateau, Phys. Rev. B **61**, 8701 (2000).

[19] K. Shiraki, T. Tsuchiya, and S. Ono, Acta Crystallogr., Sect. B: Struct. Sci **59**, 701 (2003).

[20] S. Ono, K. Hirose, N. Nishiyama, and M. Isshiki, Am. Miner **87**, 99 (2002).

[21] S. Ono, T. Tsuchiya, K. Hirose, and Y. Ohishi, Phys. Rev. B **68**, 134108 (2003).

[22] V.B. Prakapenka, G. Shen, L.S. Dubrovinsky, M.L. Rivers, and S.R. Sutton, J. Phys. Chem. Solids **65**, 1537 (2004).

[23] N. Suresh, G. Jyoti, S.C. Gupta, S.K.S. Sangeeta, and S.C. Sabharwal, J. Appl. Phys **76**, 1530 (1994).

[24] S.S. Batsanov, E. Lazareva, and L. Kopaneva, Zh. Neorg. Khim **23**, 1754 (1978).

[25] I. Rosales, C. Thions-Renero, E. Martinez, L. Bucio, and E. Orozco, High Pressure Res **31**, 428 (2011).

[26] Z. Łodziana, K. Parlinski, and J. Hafner, Phys. Rev. B **63**, 134106 (2001).

[27] K.V. Shanavas, N. Garg, and S.M. Sharma, Phys. Rev. B **73**, 094120 (2006).

[28] D. Marrocchelli, M. Salanne, and P.A. Madden, J. Phys.: Condens. Matter **22**, 152102 (2010).

[29] H. Dekura, T. Tsuchiya, and J. Tsuchiya, Phys. Rev. B **83**, 134114 (2011).

[30] Y. Tsuchida and T. Yagi, Nature **340**, 217 (1989).

[31] D. Andrault, G. Fiquet, F. Guyot, and M. Hanfland, Science **282**, 720 (1998).

[32] M. Murakami, K. Hirose, S. Ono, and Y. Ohishi, Geophys. Res. Lett. **30**, 1207 (2003).

[33] Y. Kuwayama, K. Hirose, N. Sata, and Y. Ohishi, Science **309**, 923 (2005).

[34] T. Tsuchiya and J. Tsuchiya, Proc. Natl. Acad Sci. U. S. A **108**, 1252 (2011).

[35] A.R. Oganov, M.J. Gillan, and G.D. Price, Phys. Rev. B **71**, 064104 (2005).

[36] T. Duffy, N. Madhusudhan, and K.K.M. Lee, in *Treatise on Geophysics (Second Edition)*, edited by G. Schubert (Elsevier, Oxford, 2015), pp. 149–178.

[37] C. Prescher, V.B. Prakapenka, J. Stefanski, S. Jahn, L.B. Skinner, and Y. Wang, Proc. Natl. Acad Sci. U. S. A **114**, 10041 (2017).

[38] S. Petitgirard, High Pressure Res **37**, 200 (2017).

[39] C. Meade and R. Jeanloz, Science **241**, 1072 (1988).

[40] T. Sato and N. Funamori, Phys. Rev. Lett. **101**, 255502 (2008).

[41] S.J. Tracy, S.J. Turneaure, and T.S. Duffy, Phys. Rev. Lett **120**, 135702 (2018).

[42] S. Ono, K. Funakoshi, A. Nozawa, and T. Kikegawa, J. Appl. Phys **97**, 073523 (2005).

[43] B. Zhu, C.-M. Liu, M.-B. Lv, X.-R. Chen, J. Zhu, and G.-F. Ji, Physica B **406**, 3508 (2011).

[44] B. Grocholski, S.-H. Shim, E. Cottrell, and V.B. Prakapenka, Am. Miner **99**, 170 (2014).

[45] M. Madon, P. Gillet, C. Julien, and G.D. Price, Phys. Chem. Minerals **18**, 7 (1991).

[46] S. Ono, T. Tsuchiya, K. Hirose, and Y. Ohishi, Phys. Rev. B **68**, 014103 (2003).

[47] J. Itie, A. Polian, G. Calas, J. Petiau, A. Fontaine, and H. Tolentino, Phys. Rev. Lett **63**, 398 (1989).

[48] V.V. Brazhkin, A.G. Lyapin, and K. Trachenko, Phys. Rev. B **83**, 132103 (2011).

[49] J.D. Jorgensen, J. Appl. Phys **49**, 5473 (1978).

[50] Y. Fei, A. Ricolleau, M. Frank, K. Mibe, G. Shen, and V. Prakapenka, Proc. Natl. Acad Sci. U. S. A **104**, 9182 (2007).

[51] A. Dewaele, P. Loubeyre, and M. Mezouar, Phys. Rev. B **70**, 094112 (2004).

[52] V.B. Prakapenka, A. Kubo, A. Kuznetsov, A. Laskin, O. Shkurikhin, P. Dera, M.L. Rivers, and S.R. Sutton, High Pressure Res **28**, 225 (2008).

[53] A.P. Jephcoat and S.P. Besedin, Philos. Trans. R. Soc. London, Ser. A **354**, 1333 (1996).

[54] C. Prescher and V.B. Prakapenka, High Pressure Res **35**, 223 (2015).

[55] T.J.B. Holland and S.A.T. Redfern, Mineral. Mag **61**, 65 (1997).

[56] P. Hohenberg and W. Kohn, Phys. Rev. **136**, B864 (1964).

[57] W. Kohn and L.J. Sham, Phys. Rev. **140**, A1133 (1965).

[58] S.J. Clark, M.D. Segall, C.J. Pickard, P.J. Hasnip, M.I.J. Probert, K. Refson, and M.C. Payne, Z. Kristallogr - Cryst. Mater **220**, 567 (2009).

[59] H.J. Monkhorst and J.D. Pack, Phys. Rev. B **13**, 5188 (1976).

[60] D. Vanderbilt, Phys. Rev. B **41**, 7892 (1990).

[61] C.G. Broyden, IMA J. Appl. Math **6**, 3 (1970).

[62] A.K. Singh, J. Appl. Phys **73**, 4278 (1993).

[63] A.K. Singh and T. Kenichi, J. Appl. Phys **90**, 3269 (2001).

[64] A.K. Singh, J. Appl. Phys **106**, 043514 (2009).

[65] S.M. Dorfman, V.B. Prakapenka, Y. Meng, and T.S. Duffy, J. Geophys. Res. **117**, B08210 (2012).

[66] E. Menéndez-Proupin and A.K. Singh, Phys. Rev. B **76**, 054117 (2007).

[67] P.D. Asimow, in *Treatise on Geophysics (Second Edition)*, edited by G. Schubert (Elsevier, Oxford, 2015), pp. 393–416.

[68]Supplementary Material.

[69] V.B. Prakapenka, L.S. Dubrovinsky, G. Shen, M.L. Rivers, S.R. Sutton, V. Dmitriev, H.-P. Weber, and T. Le Bihan, Phys. Rev. B **67**, 132101 (2003).

[70] T. Yoshinori, N. Yu, and T. Taku, J. Geophys. Res. B: Solid Earth **114**, (2009).

[71] A.K. Singh, H.-P. Liermann, Y. Akahama, S.K. Saxena, and E. Menéndez-Proupin, J. Appl. Phys **103**, 063524 (2008).

[72] G.Q. Chen, T.J. Ahrens, W. Yang, and J.K. Knowles, J. Mech. Phys. Solids **47**, 763 (1999).

[73] Luo. S. N, J.L. Mosenfelder, Asimow P. D., and T.J. Ahrens, Geophys. Res. Lett **29**, 36 (2002).

[74] D. Andrault, R.J. Angel, J.L. Mosenfelder, and T.L. Bihan, Am. Miner **88**, 301 (2003).

[75] B. Grocholski, S.-H. Shim, and V.B. Prakapenka, J. Geophys. Res. B: Solid Earth **118**, 4745 (2013).

[76] Y. Kuwayama, K. Hirose, N. Sata, and Y. Ohishi, Phys. Chem. Minerals **38**, 591 (2011).

[77] C. Lee and X. Gonze, J. Phys.: Condens. Matter **7**, 3693 (1995).

[78] R. Dutta, V.B. Prakapenka, and T.S. Duffy (In Preparation).

[79] S.P. Marsh, *LASL Shock Hugoniot Data* (University of California Press, 1980).

[80] G.A. Lyzenga, T.J. Ahrens, and A.C. Mitchell, J. Geophys. Res. **88**, 2431 (1983).

[81] H. Wang and G. Simmons, J. Geophys. Res. **78**, 1262 (1973).

[82] R.M. Hazen and L.W. Finger, J. Phys. Chem. Solids **42**, 143 (1981).

**Figure Captions**

Figure 1. X-ray diffraction pattern at 51.0 GPa obtained upon quenching $GeO_2$ to room temperature after heating (~1700 K). Asterisks indicate peaks from the starting $P2_1/c$ phase. The ticks at the bottom represent the expected peak positions of platinum (blue), neon (green) and α-$PbO_2$-type $GeO_2$ (red). The Miller indices of α-$PbO_2$-type germania are indicated for the corresponding peaks.

Figure 2. Experimental (red) and calculated (green) lattice parameters of α-$PbO_2$-type $GeO_2$ as a function of pressure at room temperature. Solid diamonds represent previous studies (yellow: Shiraki et al. 2003 (Ref. 19); purple: Prakapenka et al. 2003 (Ref. 69); green: Ono et al. 2003 (Ref.46)). The lattice parameters reported by Shiraki et al. 2003 (Ref. 19) were obtained from experiments performed at high-pressure and high-temperature (70.7 GPa, 2110 K).

Figure 3. Variation in unit cell volume of α-$PbO_2$-type $GeO_2$ with pressure (red: experiments; green: theory). Solid lines are 3$^{rd}$ order Birch-Murnaghan fits to the data. Other symbols are defined in Figure 2.

Figure 4. Co-variance (1σ) of the bulk modulus ($K_{0T}$) and the unit cell volume ($V_0$) (experimental data) from equation of state fitting for the α-$PbO_2$-type phase. The two different covariance ellipses represent different Pt pressure scales (solid black: Dewaele et al. 2004 (Ref. 51)/ Fei et al. 2007 (Ref. 50); dashed red: Dorfman et al. 2012 (Ref. 65)).

Figure 5. X-ray diffraction pattern at 82.8 GPa obtained upon quenching $GeO_2$ to ambient temperature after heating (~1690 K). Ticks at the bottom indicate the simulated peak positions of platinum (blue), neon (green) and $Pa\overline{3}$-type $GeO_2$ (red). Miller indices of $Pa\overline{3}$-type germania are

shown next to the corresponding diffraction peaks. Asterisks indicate peaks from the $P2_1/c$ phase.

Figure 6. Change in the unit cell volume of $Pa\bar{3}$-type $GeO_2$ as a function of pressure. Solid lines are 3rd order Birch-Murnaghan fits to the data (red: experiments; green: theory). Literature data (yellow: Shiraki et al. 2003 (Ref. 19), blue: Ono et al. 2003 (Ref. 46)) are represented by the solid diamonds.

Figure 7. Co-variance (1σ) of the bulk modulus ($K_{0T}$) and the unit cell volume ($V_0$) from equation of state fitting for the $Pa\bar{3}$-type phase (experimental data). Red and black ellipses have same meaning as in Figure 4.

Figure 8. Lattice parameter variation of platinum determined from individual (*hkl*) values at 113.9 GPa.

Figure 9. Differential stress, *t* in platinum as a function of pressure (solid blue: α-$PbO_2$ cell, solid red: $Pa\bar{3}$-type cell). The green open triangles show Pt in a neon pressure medium[65] and the black inverted triangles are for platinum in absence of a pressure medium[71]. The solid red and blue lines are linear fits to our data for the respective phases. The blue and red arrows show laser-annealing for the respective phase.

Figure 10. Theoretical Hugoniot for the rutile- (red), $CaCl_2$- (green), α-$PbO_2$- (blue) and $Pa\bar{3}$-type (yellow) $GeO_2$. Solid and dashed colored lines are for cases where γ = 1 and 2, respectively. Black circles and lines are the shock data and the fit of Jackson and Ahrens, 1979 (Ref. 1) for $GeO_2$ starting from the rutile structure. $V_0$ refers to the ambient-pressure volume of the rutile-type phase (55.33 $Å^3$). Open grey symbols are shock data for stishovite (rutile-type $SiO_2$), from Luo et al. 2002 (Ref. 73).

Figure 11. Unit cell volume of the rutile- (red), $CaCl_2$- (green), α-$PbO_2$- (blue) and $Pa\bar{3}$-type (yellow) phases of $GeO_2$ (solid) and $SiO_2$ (unfilled)[74-76]. Purple data points indicate rutile-type phase data that were not used for the EOS fit. The black and grey dashed lines indicate the phase boundaries in $GeO_2$ and $SiO_2$ respectively. The solid black lines are 3rd order Birch-Murnaghan fits to the data.

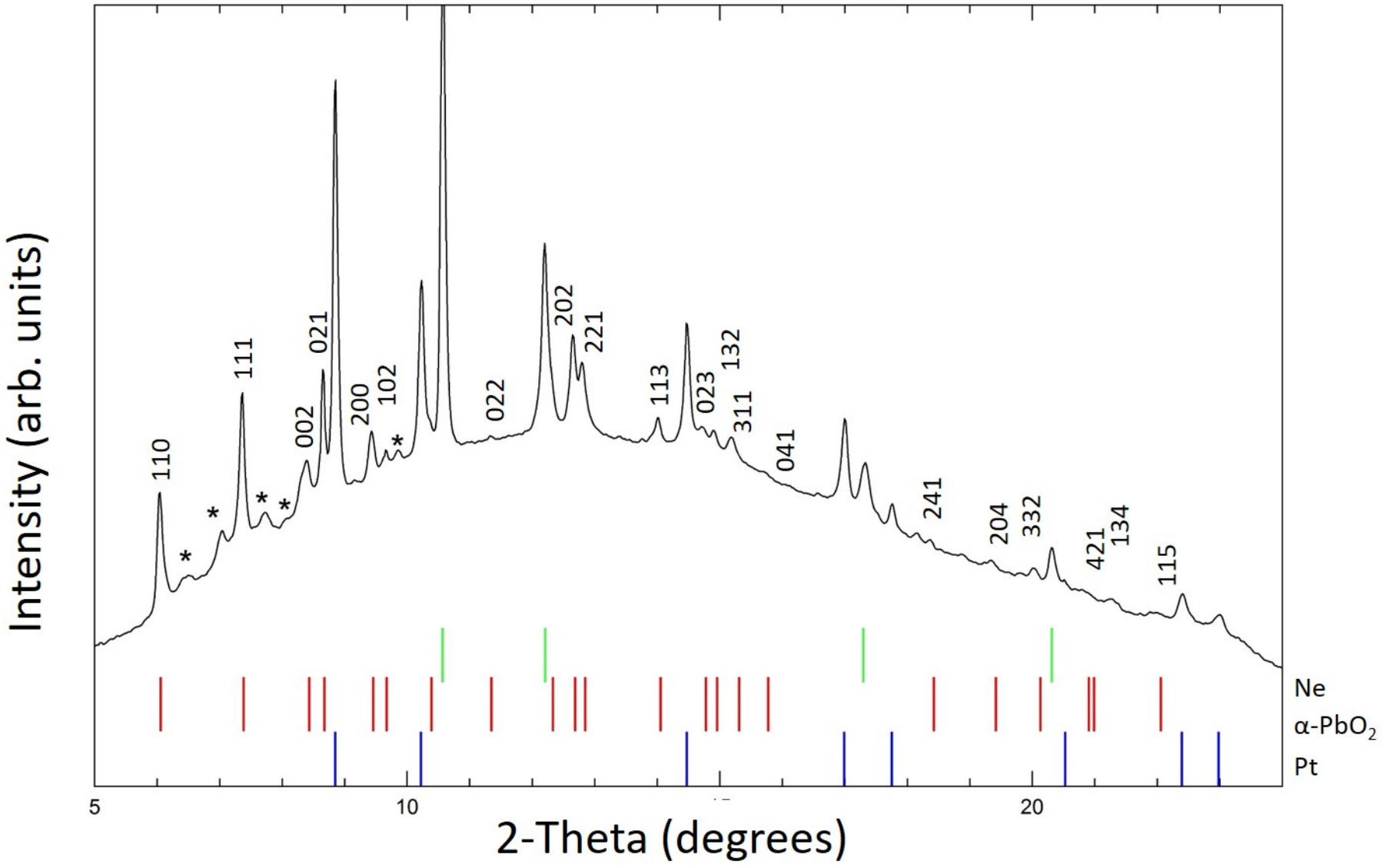
Intensity (arb. units)
110
111
002
021
200
102
022
202
221
113
023
132
311
041
241
204
332
421
134
115
Ne
α-PbO2
Pt
5
10
20
2-Theta (degrees)

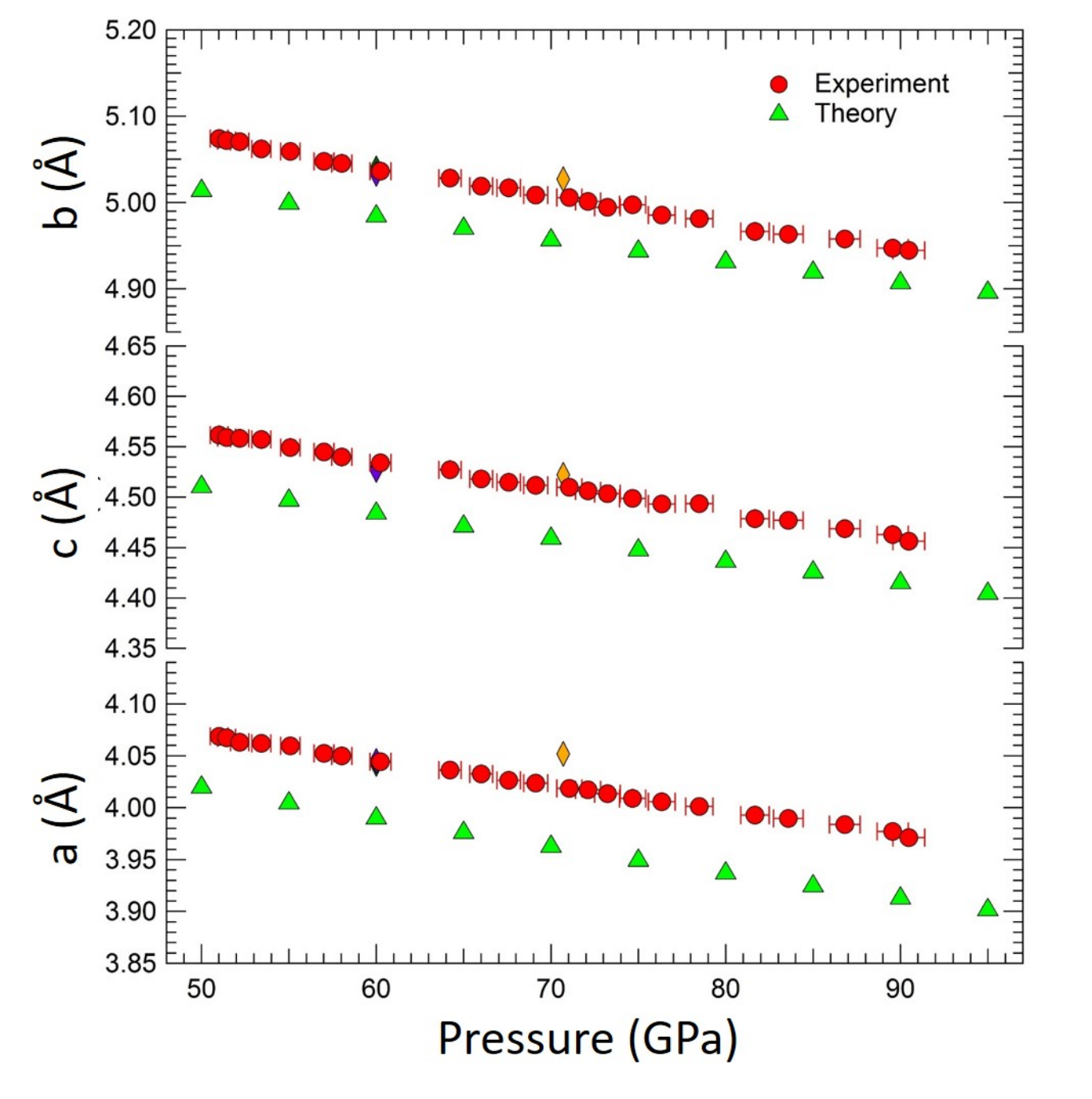
Experiment
Theory
b (Å)
c (Å)
a (Å)
Pressure (GPa)
5.20
5.10
5.00
4.90
4.65
4.60
4.55
4.50
4.45
4.40
4.35
4.10
4.05
4.00
3.95
3.90
3.85
50
60
70
80
90

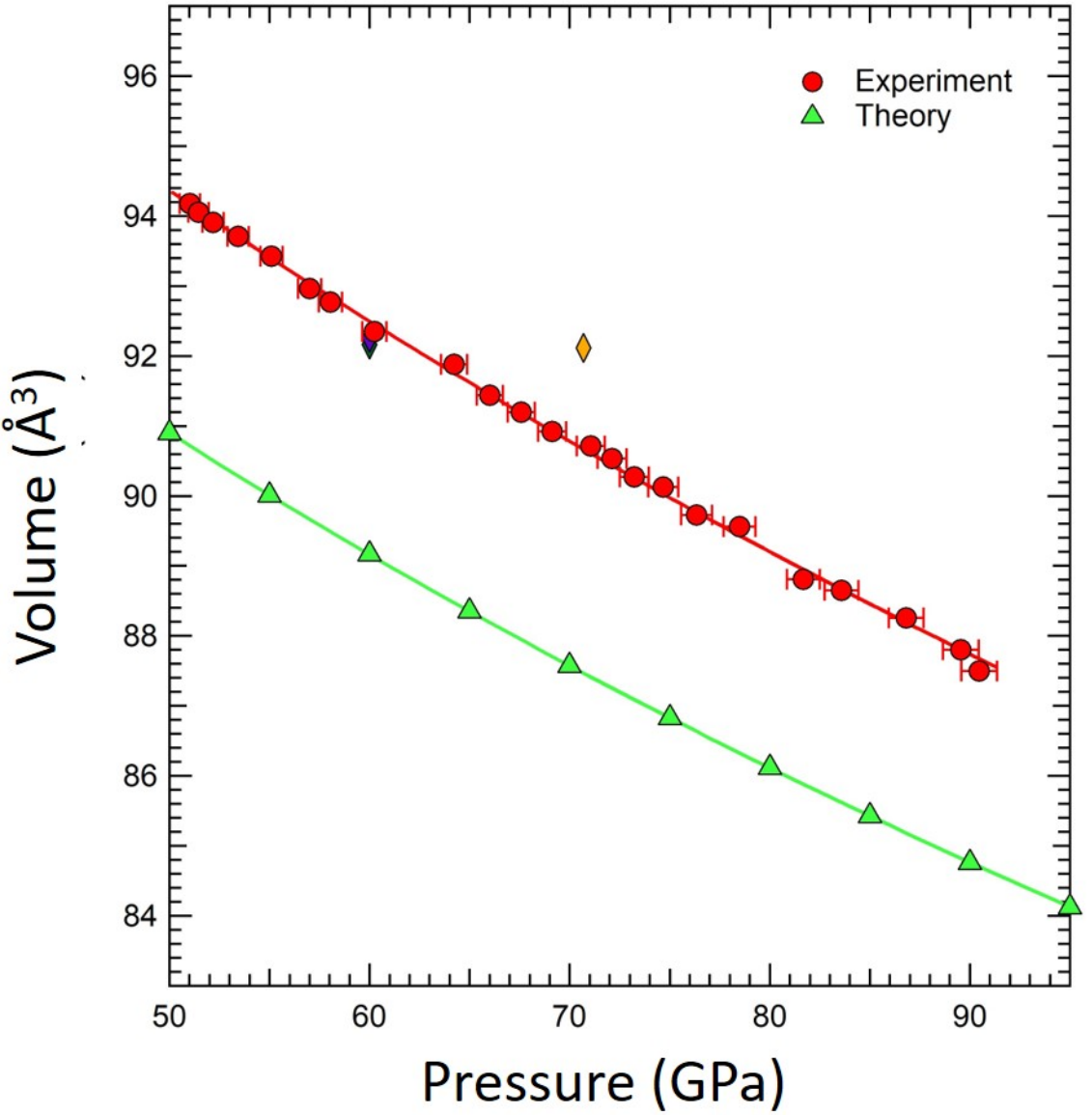
Experiment
Theory
Volume (Å³)
Pressure (GPa)
96
94
92
90
88
86
84
50
60
70
80
90

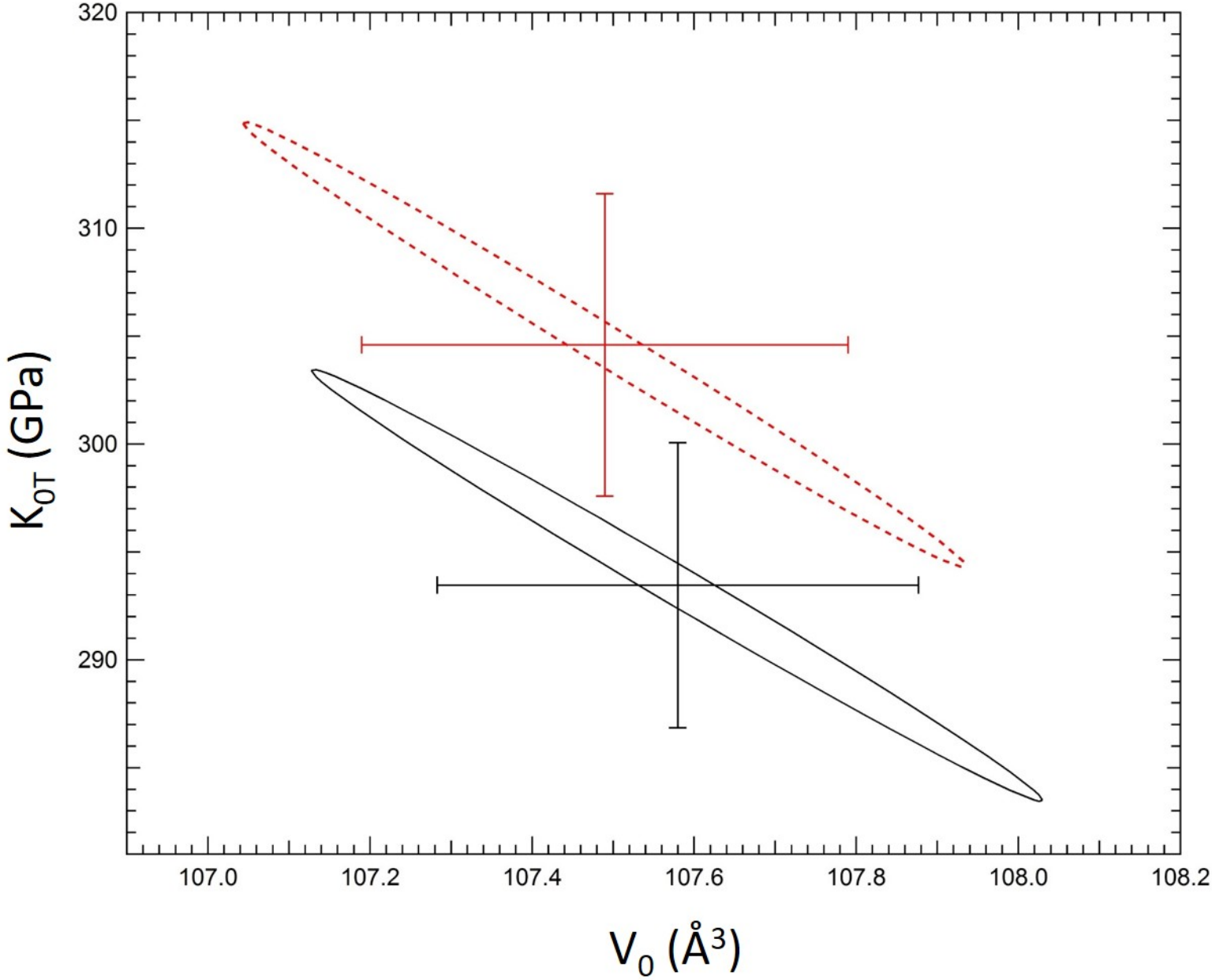
320
310
300
290
$K_{0T}$ (GPa)
107.0
107.2
107.4
107.6
107.8
108.0
108.2
$V_0$ (Å$^3$)

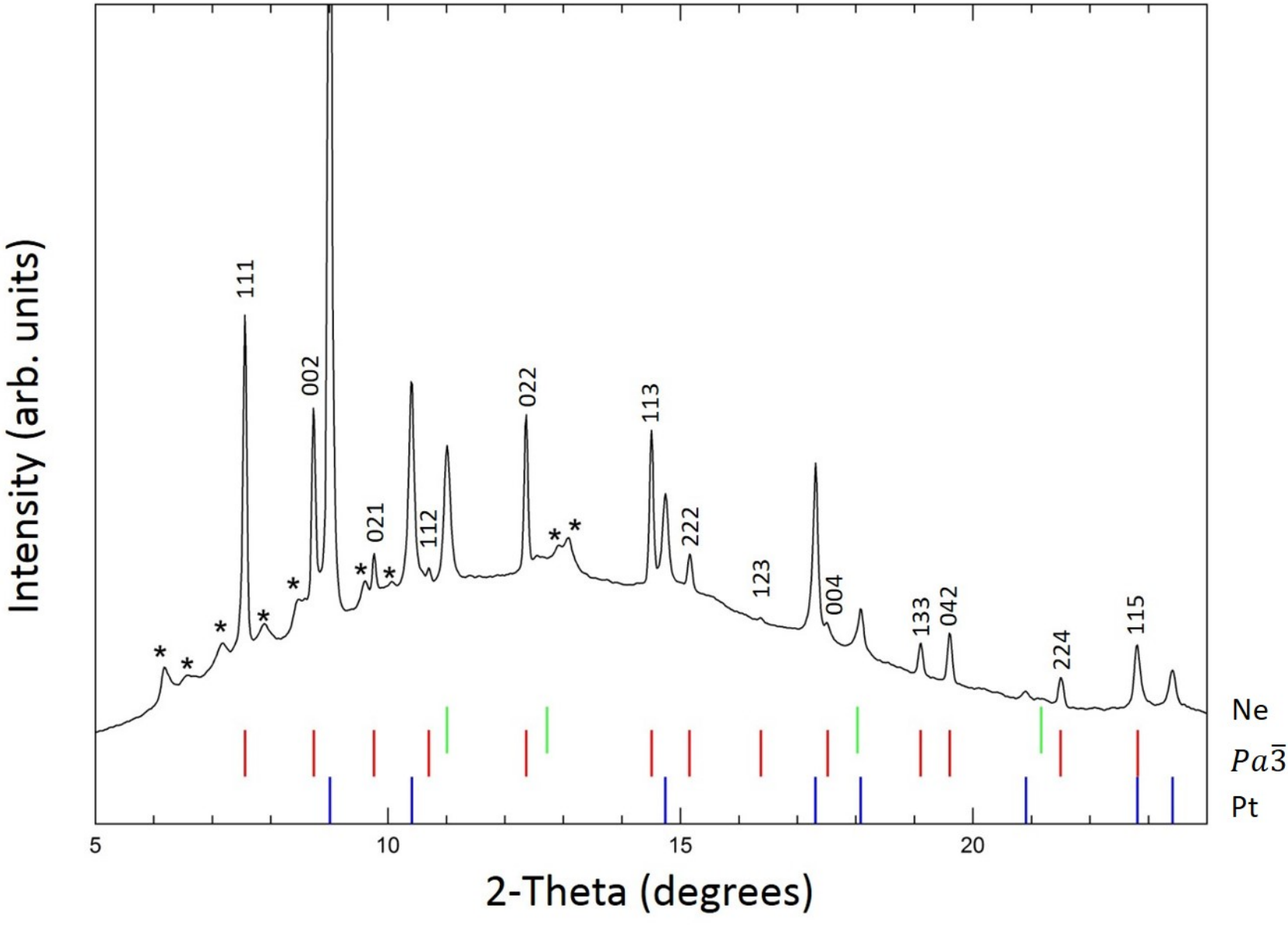
Intensity (arb. units)
111
002
021
112
022
113
222
123
004
133
042
224
115
*
5
10
15
20
2-Theta (degrees)
Ne
$Pa\bar{3}$
Pt

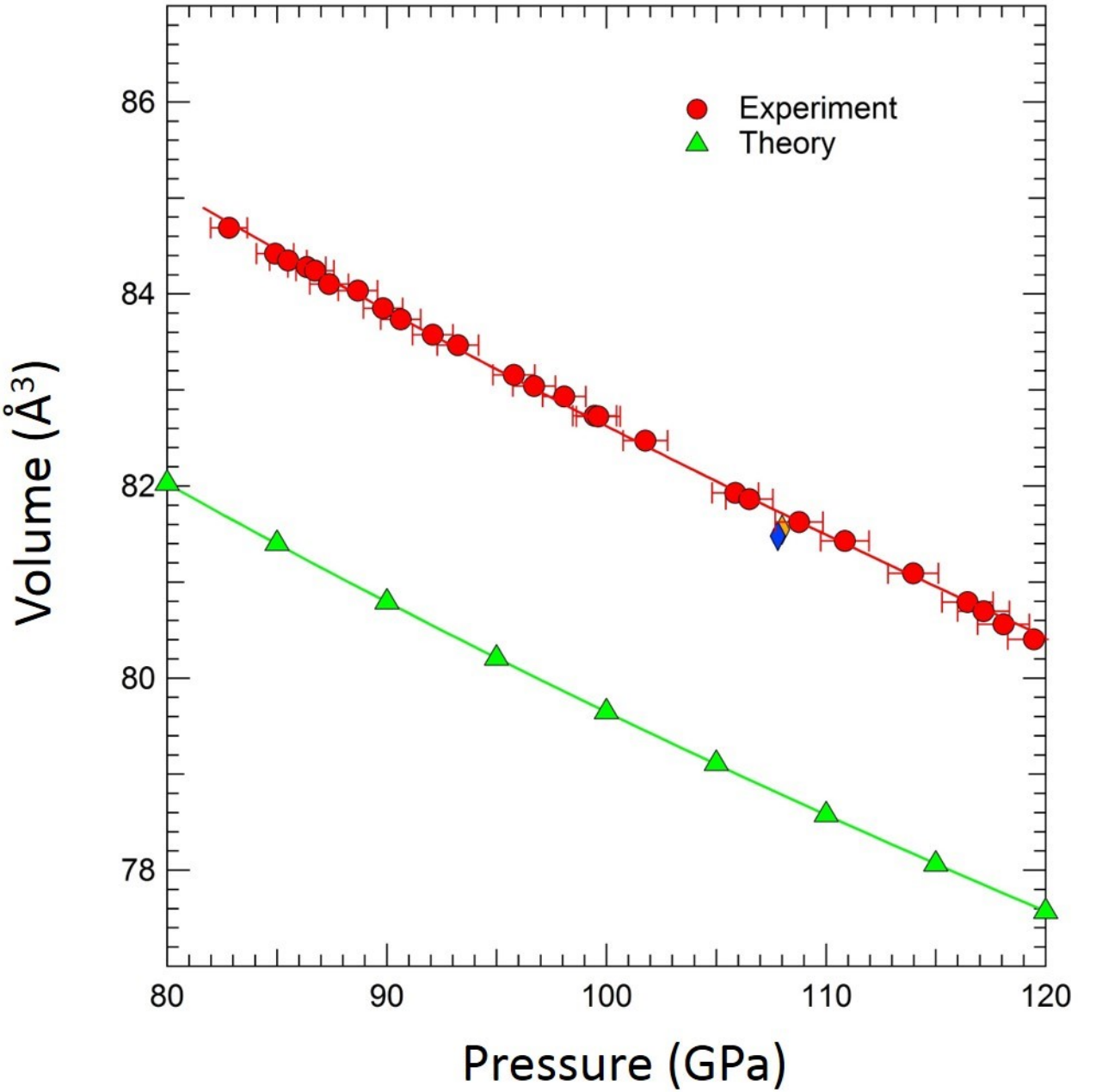
Experiment
Theory
Volume (Å$^3$)
Pressure (GPa)
86
84
82
80
78
80
90
100
110
120

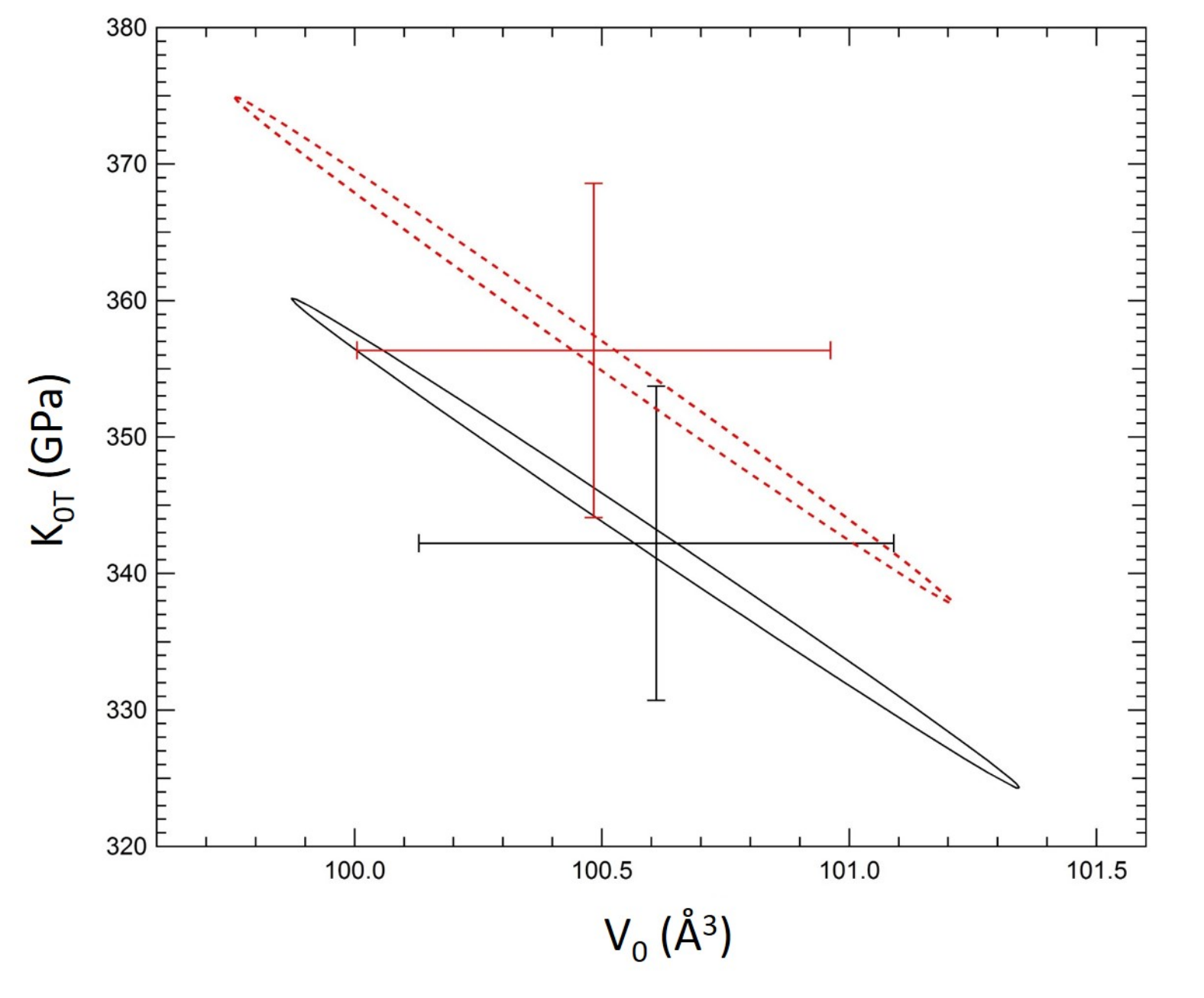
380
370
360
350
340
330
320
100.0
100.5
101.0
101.5
$K_{0T}$ (GPa)
$V_0$ (Å$^3$)

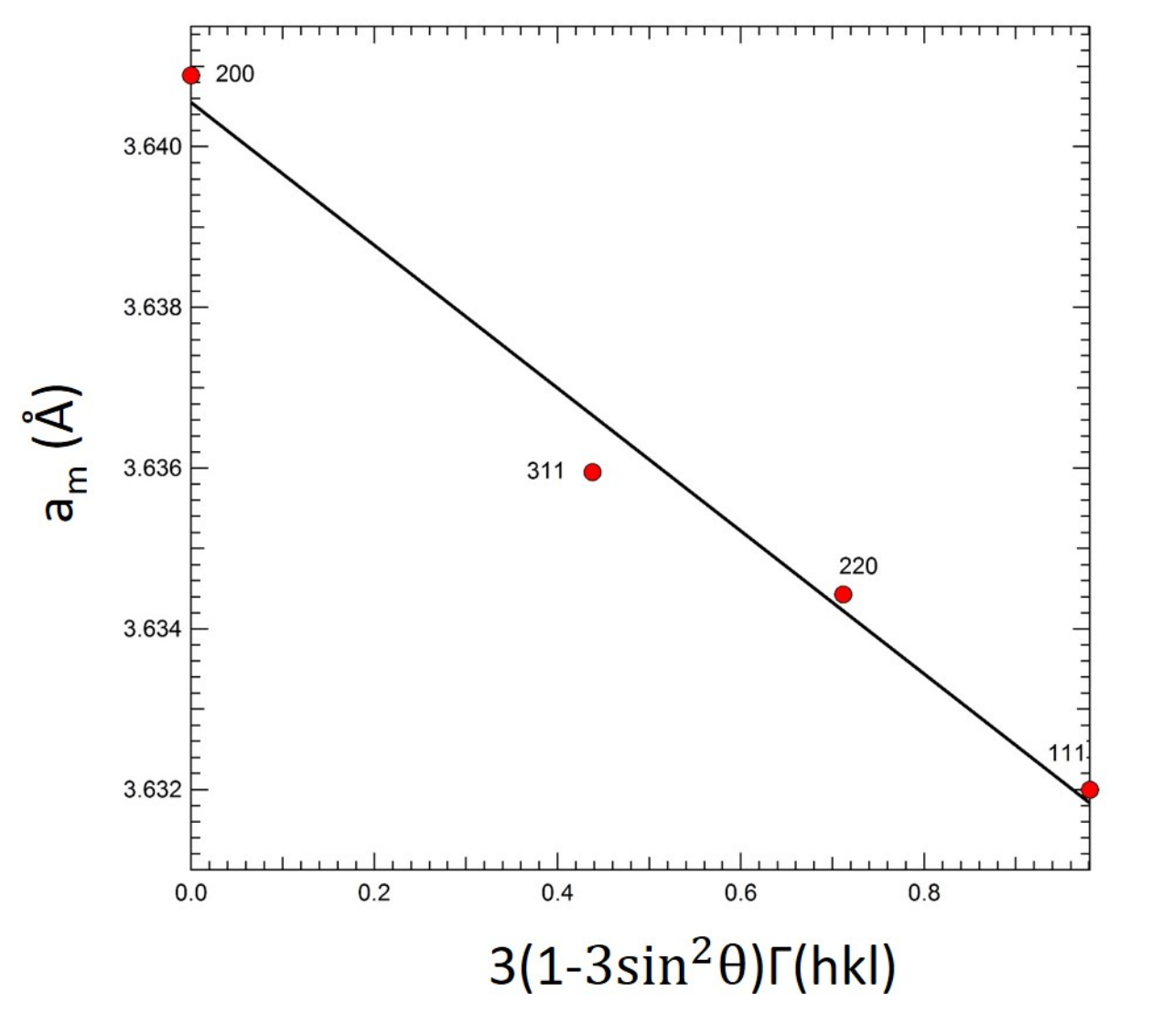
200
311
220
111
3.640
3.638
3.636
3.634
3.632
0.0
0.2
0.4
0.6
0.8
$a_m$ (Å)
$3(1-3\sin^2\theta)\Gamma(hkl)$

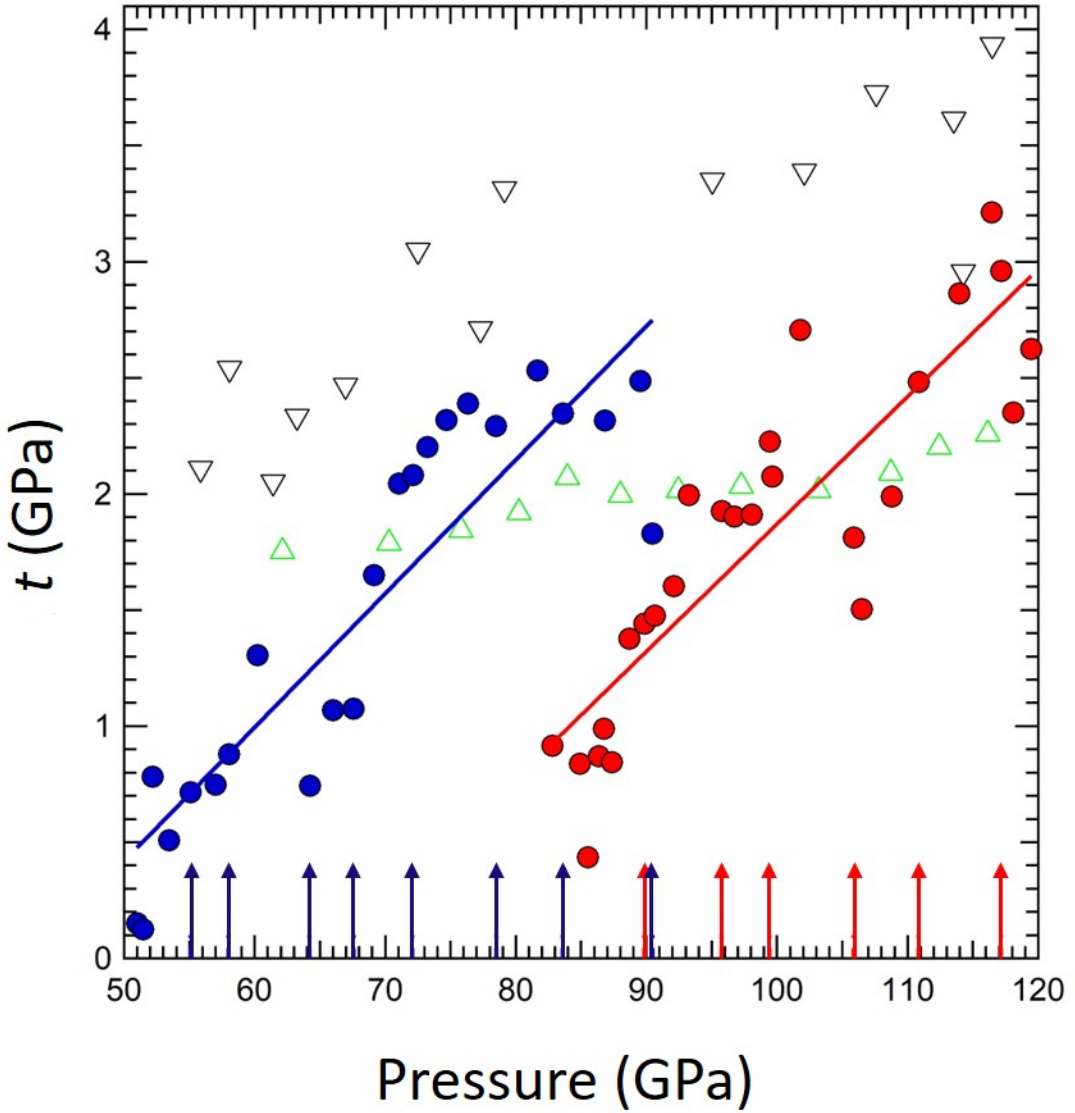
t (GPa)
Pressure (GPa)
0
1
2
3
4
50
60
70
80
90
100
110
120

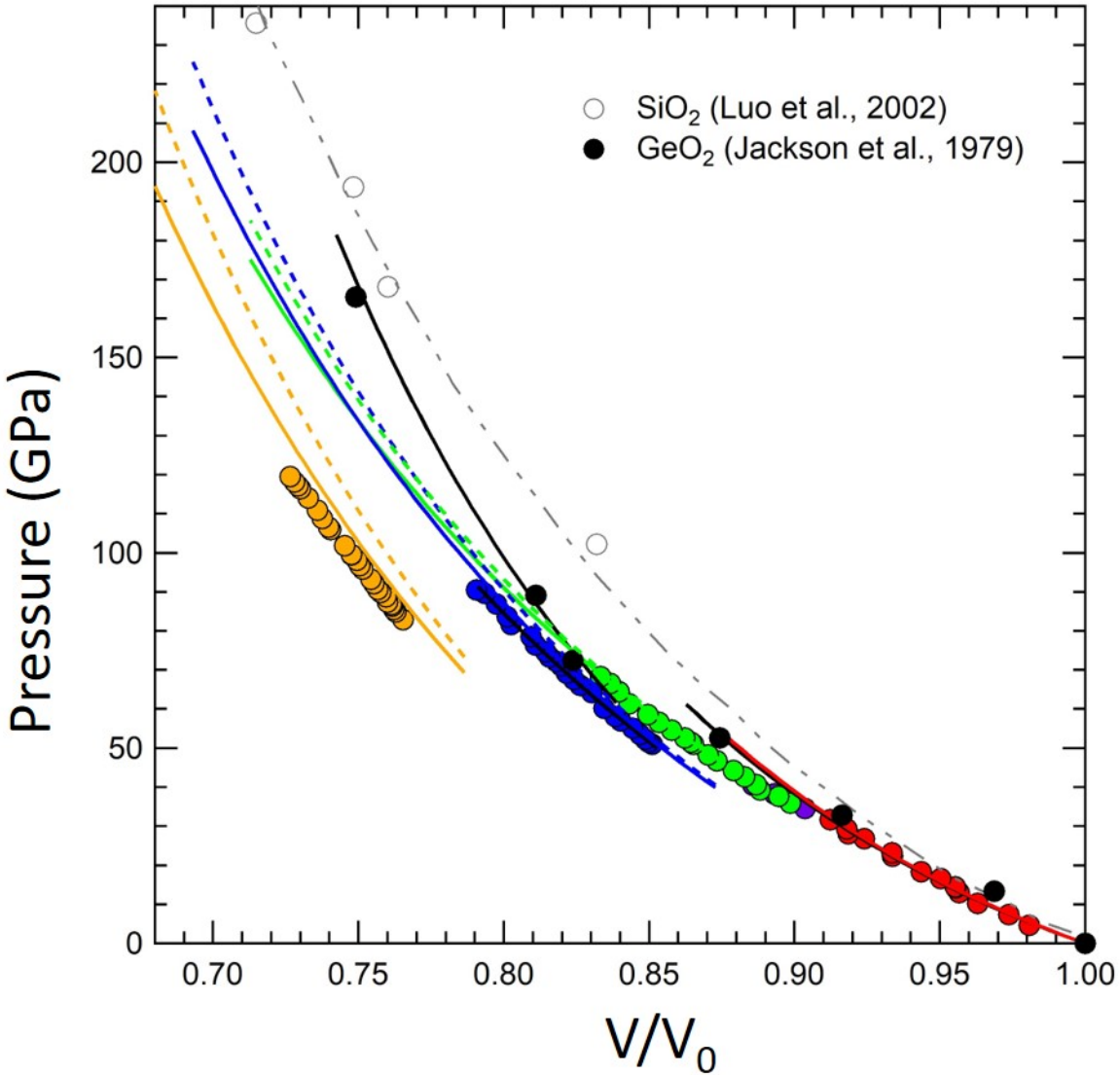
SiO2 (Luo et al., 2002)
GeO2 (Jackson et al., 1979)
Pressure (GPa)
0
50
100
150
200
0.70
0.75
0.80
0.85
0.90
0.95
1.00
V/V0

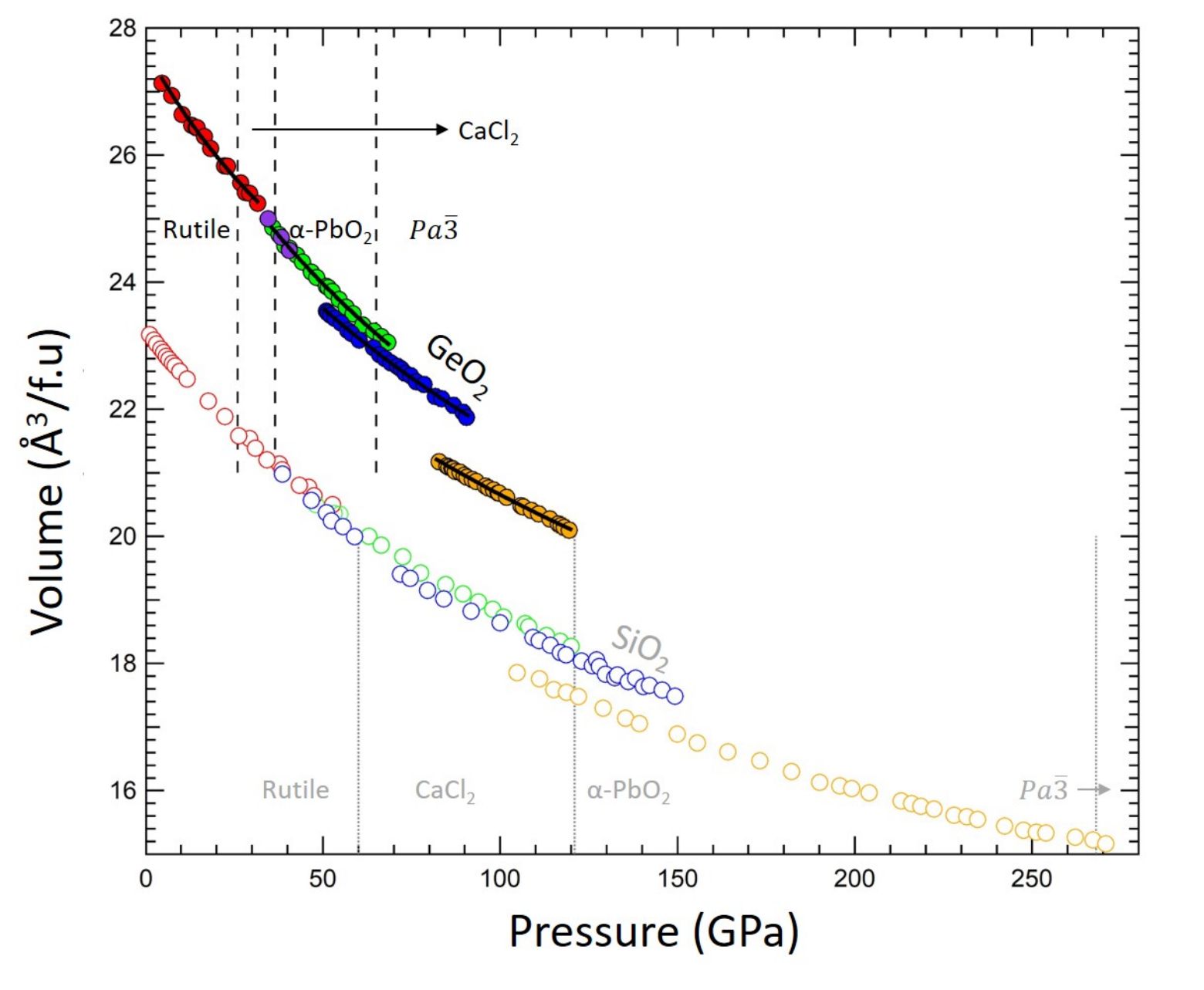
Volume (Å³/f.u)
Pressure (GPa)
28
26
24
22
20
18
16
0
50
100
150
200
250
CaCl2
Rutile
α-PbO2
Pa3̄
GeO2
SiO2
Rutile
CaCl2
α-PbO2
Pa3̄

Table 1. Equation of state parameters of the α-$PbO_2$- and $Pa\overline{3}$-type phases of $GeO_2$ and $SiO_2$.

| Phase | $GeO_2$ (This Study) | | | | $SiO_2$ | | |
|---|---|---|---|---|---|---|---|
| | Method | $V_0$ (Å$^3$) | $K_{0T}$ (GPa) | $K'_{0T}$ | $V_0$ (Å$^3$) | $K_{0T}$ (GPa) | $K'_{0T}$ |
| α-$PbO_2$ | Experiment | 53.8 (2)[a] | 293 (7)[a] | 4[a] (fixed) | 45.8[a] | 322 (2)[a] | 4[a] (fixed) |
| | LDA | 51.7[a] | 291[a] | 4.4[a] | 45.56[b] | 324[b] | 4.2[b] |
| | | 51.6[a] | 307[a] | 4[a] (fixed) | | | |
| $Pa\overline{3}$ | Experiment | 50.3 (3)[a] | 342 (12)[a] | 4[a] (fixed) | 43.6 (2)[c] | 348 (5)[c] | 4[c] (fixed) |
| | LDA | 48.8[a] | 313[a] | 4.4[a] | 43.5[b] | 345[b] | 4.3[b] |
| | | 48.3[a] | 351[a] | 4[a] (fixed) | | | |

[a] Grocholski et al. 2013 (Ref. 75); [b]Oganov et al. 2005 (Ref. 35); [c]Kuwayama et al. 2011 (Ref. 76).

LDA = local density approximation.

Table 2. Thermodynamic parameters of $GeO_2$ used for the calculation of the theoretical Hugoniot.

| Phase | $\boldsymbol{\gamma_0}$ | $q$ | α ($10^{-5}K^{-1}$) | $E_{TR}$ (kJ/g) |
|---|---|---|---|---|
| Rutile | 1.16[a] | 1* | 2.03[a] | -- |
| $CaCl_2$ | 1, 2* | 1* | 2.05* | 0 |
| α-$PbO_2$ | 1, 2* | 1* | 2.05* | +0.07 |
| $\boldsymbol{Pa\bar{3}}$ | 1, 2* | 1* | 2.05* | +0.21 |
| Hpp[c] | 1.24[c] | 0[c] | | +0.1[c] |

*Assumed value, Hpp: high-pressure phase observed on shock compression[1] of rutile-type $GeO_2$, γ: Grüneisen parameter, α: thermal expansion coefficient, $E_{TR}$: phase transition energy. The subscript 0 indicates zero-pressure conditions.

[a]Wang and Simmons, 1973 (Ref. 81); [b]Hazen and Finger, 1981 (Ref. 82); [c]Jackson and Ahrens, 1979 (Ref. 1).